Published in final edited form as:
IEEE J Sel Top Quantum Electron. 2014 ; 20(3): 6900806–. doi:10.1109/JSTQE.2014.2301016.

Surface-Enhanced Raman Spectroscopy Sensors From Nanobiosilica With Self-Assembled Plasmonic Nanoparticles

Fanghui Ren [Student Member, IEEE],
Oregon State University Corvallis, OR 97331 USA

Jeremy Campbell,
School of Chemical, Biological, and Environmental Engineering Oregon State University Corvallis, OR 97331 USA

Gregory L. Rorrer, and
School of Chemical, Biological, and Environmental Engineering Oregon State University Corvallis, OR 97331 USA

Alan X. Wang
Department of Electrical Engineering and Computer Science, Oregon State University, OR 97331 USA

Fanghui Ren: renf@onid.orst.edu; Jeremy Campbell: campbjer@onid.orst.edu; Gregory L. Rorrer: rorrergl@engr.orst.edu; Alan X. Wang: wang@eecs.oregonstate.edu

Abstract

We present an innovative surface-enhanced Raman spectroscopy (SERS) sensor based on a biological-plasmonic hybrid nanostructure by self-assembling silver (Ag) nanoparticles into diatom frustules. The photonic-crystal-like diatom frustules provide a spatially confined electric field with enhanced intensity that can form hybrid photonic-plasmonic modes through the optical coupling with Ag nanoparticles. The experimental results demonstrate 4–6× and 9–12× improvement of sensitivities to detect the Raman dye for resonance and nonresonance SERS sensing, respectively. Such low-cost and high-sensitivity SERS sensors have significant potentials for label-free biosensing.

Index Terms

Diatom frustules; surface plasmons; photonic crystals; surface-enhanced Raman spectroscopy

I. Introduction

Surface-enhanced Raman spectroscopy (SERS) has been widely investigated as an analytical tool for the detection of various biological and chemical molecules with single molecular sensitivity due to the strong electric fields induced by plasmonic resonances [1], [2]. Even though an enhancement factor (EF) as large as 10^{14} has been report by comparing the measured SERS cross-section of a molecule in the hot-spot to a typical Raman scattering cross-section, controlling the location and density of such hot-spots remains a major challenge for reliable SERS sensing [3], [4]. Moreover, increasing the average EF of the whole SERS substrate is even more desirable than obtaining a few extremely strong but very

rare hot spots, as the former device can increase the detection probability while reducing the excitation laser power and the integration time for high-throughput optical sensing applications. It has been theoretically proved and experimentally confirmed that placing metallic nanoparticles (NPs) near or inside dielectric microcavities can form hybrid photonic-plasmonic modes [5], [6], which will further increase the quality-factors and the local electric field. This concept has been successfully applied to SERS sensing by decorating dielectric ring resonators and photonic crystals with metallic NPs [7]–[9]. In these hybrid nanostructures, the guided-mode resonances (GMRs) of the photonic crystal slab efficiently couple to the localized surface plasmons (LSPs) of the metallic nanostructures, resulting in a higher local electric field to enhance the SERS signals. However, such artificial photonic crystals require top-down fabrication techniques such as optical lithography and reactive-ion etching (RIE) [10]. Conventional bottom-up bioprocess, such as cell cultivation, provides an alternative approach of fabricating nanoscale structure with low cost and less complexity.

Nature may provide abundant and inexpensive sources for photonic-crystal-like structures. Diatoms are photosynthetic marine micro-organisms that create their own skeletal shells of hydrated amorphous silica, called frustules, which possess hierarchical nano-scale photonic crystal features [11], [12]. Such nano-biosilica is formed by a bottom-up approach at ambient temperature and pressure when a diatom takes up water soluble silicic acid from the environment, which is precipitated into amorphous silica within an intracellular nano-bioreactor. Diatom frustules are low-cost, nanoscale, and hierarchically structured materials that could potentially revolutionize the fabrication of photonic crystals. Potential applications of diatoms for the detection of antibodies, solar cells, electroluminescent display, high surface area battery materials, photoluminescence, and nanoplasmonic photonic devices have been explored by many researchers [13]–[19]. Our previous work theoretically and experimentally demonstrated that the photonic-crystal-like structure of a diatom frustule can provide GMRs in the visible wavelength range [20]. NPs-on-diatom nanostructures provide enhanced plasmonic resonances at visible wavelengths due to the intrinsic surface plasmonic resonances of silver (Ag) NPs coupled with the GMRs of diatom frustules [20]. Such NPs-on-diatom nanostructures with enhanced LSPs are expected to have a tremendous engineering potential for SERS sensors.

In this paper, we systematically investigate the application of the NPs-on-diatom nanostructure for SERS sensing. By coating Ag NPs onto diatom frustules using a self-assembly method, we observe enhanced SERS signals due to the coupling of the LSPs with the GMRs of the photonic structure of the diatom frustules. Stronger optical scattering was directly observed from the NPs on a diatom than that on the glass substrate via a high magnification microscope. SERS detection of Rhodmine 6G (R6G) molecules at resonance wavelength (532 nm) shows that the NPs-on-diatom structure provides 4–6× improvement in sensitivity when compared to the NPs-on-glass structure that is confirmed by confocal SERS mapping. When excited by non-resonance wavelength (785 nm), the NPs-on-diatom structure provides 9–12× improvement in SERS sensitivity.

II. Sample Preparation

A. Diatom Fabrication

Pinnularia sp. is a single-celled marine diatom with an elliptical cell shape. A representative scanning electron microscopy (SEM) image of the diatoms is presented in Fig. 1(a). The cell dimensions for this species are ~30 μm along the major axis and ~5 μm along the minor axis. Biogenic silica materials were grown on glass substrates and the organic cell materials were removed. The details of the cell cultivation of diatom frustules can be found in our previous work [20]. The structure of a diatom frustule with submicron features is shown in the SEM image in Fig. 1(b). The diatom frustule consists of two-dimensional arrays of sub-micron pores with diameters of ~200 nm. The primary pores of the frustule were lined with a thin layer of biosilica containing several subpores with diameters of 25–50 nm. The nominal lattice constant of the nanophotonic structure is 340 ± 30 nm with refractive index ranging between 1.43 and 1.48 [12].

B. Silver Self-Assembly to Amine-Functionalized Diatom Biosilica

The Ag NPs solution was prepared by the Lee-Mesel Method [21]. 250 mL of 1 mM silver nitrate aqueous solution was heated to boiling in an oil bath. Sodium citrate (1%, by weight) solution of 5 mL was added to the silver nitrate solution as soon as the boiling occurred, and heating condition was continued for an additional 1 h. The color of the solution turned into grayish yellow which indicated that the reaction was completed.

The Ag NPs were self-assembled onto a diatom-coated glass substrate modified with aminopropyltriethoxylsilane (APTES) [22]. First, the substrate was immersed in a RCA solution (1:1:5 $H_2O_2/NH_4OH/H_2O$) for 1 h at 70 °C. The sample was then rinsed with deionized water and methanol. This pretreatment created abundant hydroxyl groups on the diatom frustule and the substrate surface. After cleaning, the diatom samples were immersed in APTES (10%, by weight in methanol) solution for 5 h, followed by rinsing with copious methanol and deionized water. The APTES was attached to the sample surface by the hydroxyl groups created from the previous treatment. The sample was immersed into an Ag colloidal suspension overnight (12 h) and rinsed with deionized water and dried with high-purity nitrogen

Ag colloids prepared by the Lee-Mesel method yield Ag NPs with a wide range of sizes (50–150 nm), geometries and aggregation states. NPs of various aggregation states including isolated NPs, NP dimers, trimers, short chains, and nanorods are distributed on top of the frustule and substrate respectively, as shown in Fig. 2(a) and (b). It has been studied that the nanoparticle size and shape are less crucial than the size of interparticle gaps in the SERS measurement [23]. Previous studies suggest that the enhancement factors for the NPs significantly depend on the formation of optical hot-spots, where two particles are in a few nanometers proximity [23], [24], which were randomly formed on diatom frustules and the glass substrate, as shown in the SEM images. Fig. 2(c) and (d) show the high-magnification optical microscopy images focused on a diatom frustule and on the glass substrate, respectively. These images directly compare the optical scattering from the Ag NPs on the

diatom frustule and the Ag NPs on the flat glass substrate, which suggest that the LSPs are significantly enhanced by the diatom frustule.

III. Results and Discussion

A. SERS Measurement Under Resonance Condition

In order to evaluate the sensitivity of the SERS sensor based on nanobiosilica with self-assembled Ag NPs, spectra of R6G molecules were collected using the excitation light at molecular resonance wavelength (532 nm) and nonresonance wavelength (785 nm) on the NPs-on-diatom and NPs-on-glass samples, respectively. R6G is a strong fluoresce dye which shows a molecular resonance Raman scattering effect with the excitation wavelength at 532 nm. In our SERS measurement, R6G molecules in ethanol were drop-coated on the glass substrate with diatom frustules and then evaporated to dryness. Molecular resonance SERS microscopy was performed using a Horiba Jobin-Yvon HR800 confocal Raman spectrometer equipped with a 532 nm diode laser through a notch filter. During the measurement, the confocal pin-hole size was set at 100 μm. A 50× objective lens (NA = 0.75) was used to focus the excitation light to a 2 μm spot totally within a single diatom frustule for each spectrum acquisition. Raman signals were detected by a Synapse charge-coupled device (CCD) detector. Fig. 3(a) shows the single-point SERS signals measured on the flat glass substrate and on the diatom frustule, respectively. SERS signals of the NPs-on-diatom structure show 3.6–6.2× enhancement compared with that on the NPs-on-glass substrate for major R6G Raman peaks at 614, 1368, 1511, 1578, and 1651 cm^{-1}. The additional enhancement of Raman signals is attributed to the enhanced LSPs due to the presence of the diatom frustule. R6G Raman spectra have been studied in the concentration range of 10^{-9} to 10^{-4} M. The Raman band at 1368 cm^{-1} was used to probe the strength of the SERS of which the intensity were plotted in Fig. 3(b). The Raman signals increase from 10^{-8} M to 10^{-5} M after which the Raman intensity decreases at 10^{-4} M. 4.1–6.4× enhancement factors of the Raman signals between the NPs-on-diatom and the NPs-on-glass samples were observed throughout the concentration range of 10^{-8} to 10^{-5} M, which are attributed to the GMRs of the diatom frustule. When further increasing the concentration from 10^{-5} to 10^{-4} M, more R6G molecules were attached to the nano-corrugated surface of the frustule, which resulted in a significant increase of florescence baseline. In this case, the florescence signals competed with the SERS signals and degraded the SERS intensity. Therefore, the decreasing of Raman signal intensity was observed after subtracting the florescence baselines when we increased the R6G molecules to a higher concentration above 10^{-4} M.

The intensity of SERS signals depend on the local R6G concentration, the aggregation states of the Ag NPs, and the surfaces of diatom frustules. By mapping a large area of the substrate which includes a diatom frustule as well as some flat glass surface, we are able to investigate the average effects of these factors on SERS signal intensity. A total of 625 SERS spectra were acquired within the scanning range of 50 μm × 50 μm that is divided into an acquisition area of 25 × 25 grids, as shown in Fig. 3(c) and (d). The SERS mapping results of the intensity of 1368 cm^{-1} Raman peak exhibit a pattern of increased signal intensity which correlates with the shape of the diatom frustule that is observed in the corresponding

optical image. The average measured SERS signal intensity for the NPs-on-diatom area was 1745 ± 1275 counts/(mW·s), whereas the average signal intensity of the NPs-on-glass area was 406 ± 393 counts/(mW·s). The presence of the diatom photonic structures results in an average SERS-EF of 4.3× compared to that on the flat glass substrate. This SERS mapping measurement suggests that highly enhanced surface plasmons are localized on the diatom frustules, achieving a diatom-based SERS sensor that can substantially enhance the SERS sensitivity. The EF was strongly correlated to the enhanced electric field around the Ag NPs due to the GMRs of the photonic crystal structure.

In order to verify whether the additional enhancement of Raman signals comes from the photonic crystal structure of the diatom frustules, we mapped the Raman signals with respect to the NPs density. Such analysis will rule out the effect of NP density variation on diatom and glass substrate [25], [26]. SERS mapping signals were collected in a deterministic acquisition area as shown in a SEM image in Fig. 4(a), from which the NP density can be accurately obtained. To prepare the sample, the NP solution was diluted by 1:10 with water. Due to the relatively large sizes of the Ag NPs, the NPs were excluded from the nanopores and were majorly assembled on the surface of the diatom frustules. The SEM image shows that in the SERS mapping area, Ag NPs were uniformly distributed onto the diatom and glass substrate with an average density of $7/\mu m^2$. This conclusion is also confirmed by the zoomed SEM images as shown in Fig. 2(a) and (b), which show that there is no statistic difference of the NP density and morphologies between the glass and diatom substrate. A SERS map of 6 × 6 grids (36 mapping points, grid size: 2 μm) for R6G was acquired. The Raman peak at 1368 cm^{-1} was analyzed to generate the map and the mapping intensities were normalized by the NP densities in each grid, which are shown in Fig. 4(b). The diatom photonic crystal structure results in an average SERS EF of 3.8× when compared to that on the flat glass substrate. In some area, the EF can be as high as 7.2×. Therefore, it is unequivocal to conclude that the GMR effect of diatom frustules can enhance the SERS signals.

B. SERS Measurement Under Nonresonance Condition

SERS spectra were recorded using 785 nm excitation wavelength to avoid a complex interference of molecular resonance Raman scattering effect since the excitation energy of 785 nm is away from the electronic absorption band of R6G, which results in nonresonance Raman scattering. Due to the fact that the glass substrate displays strong florescence background under the 785 nm wavelength excitation, diatom frustules in aqueous solution were drop-coated on non-florescent quartz substrate for the measurement. The diatom frustules were annealed at 425 °C in air for 1 h in order to improve the adhesion to the quartz substrate. The fabrication process of self-assembled NPs onto a diatom-coated quartz substrate is identical to the diatom-coated glass substrate as described in Section II. Fig. 5(a) shows the nonresonance SERS spectra under the 785 nm excitation light from a diode laser. The SERS spectra indicates that the Raman signal intensity is enhanced by 8.7–13.3× on the diatom frustule compared with the flat quartz substrate for the Raman bands of 776, 1183, 1315, 1368, and 1511 cm^{-1}. The larger additional enhancement factors from diatom frustules to the R6G Raman signals under nonresonance condition compared with resonance condition can be explained by the difference between resonance and nonresonance Raman

scattering by surface plasmons [27]. Resonance Raman process is subjected to quenching effect, where an additional loss is introduced for the energy stored in coherent oscillations of molecular dipoles at the excitation wavelengths in the presence of LSP enhancement and GMR enhancement [27]. Compared with resonance Raman process which limits the attainable enhancement, such quenching effect is absent in normal nonresonance Raman scattering.

The intensities of the Raman band at 1368 cm^{-1} were plotted in the concentration ranges from 10^{-7} M to 10^{-3} M in Fig 5(b). The average enhancement effect to the Raman signals was observed throughout the concentration range of 10^{-7} to 10^{-4} M with enhancement factors of 8.9–12.3× between NPs-on-diatom and NPs-on-quartz. For the SERS mapping measurement, an area of 15 μm × 15 μm in Fig. 5(c) was scanned to generate a map in Fig. 5(d). The average measured SERS signal intensity for the NPs-on-diatom area was 33.2 ± 21.8 counts/(mW·s), which shows an average signal enhancement of 9.2× compared to quartz substrate whereas the average signal intensity of the NPs-on-quartz area was 3.63 ± 2.48 counts/(mW·s). Such EF for nonresonance SERS is more desirable for biosensing application as fluorescence interference can be avoided compared with resonance SERS.

C. Evaluation of Guided Mode Resonance From Diatom Frustules

Our previous research presented the GMRs from diatom frustules by measuring the extinction spectrum at visible wavelengths [20], which shows a broad, low-Q resonance that can be coupled with the plasmonic resonances of Ag NPs. In order to confirm the effective enhancement at both 532 nm and 785 nm, a broadband white light source with Vis-NIR (visible to near infrared) output was used as the excitation source. Details of the experimental setup can be found in Ref [20]. From the extinction spectra as shown in Fig. 6(a), the diatom frustule increases the optical extinction ratio of the NPs by 2× compared to Ag NPs on the glass substrate from 500 nm to 850 nm wavelength.

The Raman scattering signals of R6G molecules on the diatom and the glass substrate were also investigated respectively without plasmonic enhancement from NPs in order to confirm the contribution of GMRs from diatom frustules. Raman signals of 5 mM R6G from the diatom frustule (black) and glass substrate (red) are plotted in Fig. 6(b). The amplitude of the Raman signals is very weak, but it still clearly shows that there is 3.9 × enhancement for the Raman peak at 1368 cm^{-1} from the diatom frustule compared to that from the glass substrate. We attribute this enhancement to the GMRs of the diatom frustules.

IV. Conclusion

In conclusion, we have demonstrated that the GMRs of diatom frustules can effectively couple with the LSPs of the Ag NPs, which will increase the average EF of SERS sensors. An additional EF of the SERS signals of 4–6× was observed for resonance condition when the molecular concentrations are from 10^{-9} to 10^{-5} M. Under nonresonance condition, the Raman EF of 9–12× was obtained over the concentrations from 10^{-7} M to 10^{-4} M. Such NPs-on-diatom SERS substrate will have significant potentials in chemical and biochemical diagnostics, pathogen detection, and environmental protection.

Acknowledgments

The work of A. X. Wang was supported by Marine Polymer Technologies, Inc. The work of F. Ren was supported by the National Institute of Health under Grant 9R42ES024023-02. The work of G. L. Rorrer was supported by the National Science Foundation through the Emerging Frontiers in Research and Innovation (EFRI) program under Award 1240488.

The authors would like to thank X. Wang for the help of taking SEM images of the samples.

References

1. Homola J, Yeea SS, Gauglitzb G. Surface plasmon resonance sensors: Review. Sens Actuators, B. Jan.1999 54:3–15.
2. Vo-Dinh T. Surface-enhanced Raman spectroscopy using metallic nanostructures. TrAC, Trends Anal Chem. Sep; 1998 17(8):557–582.
3. Kneipp K, Wang Y, Kneipp H, Perelman LT, Itzkan I, Dasari R, Feld MS. Single molecule detection using surface-enhanced Raman scattering (SERS). Phys Rev Lett. Mar.1997 78:1667–1670.
4. Nie S, Emory SR. Probing single molecules and single nanoparticles by surface-enhanced Raman scattering. Science. Feb; 1997 275(5303):1102–1106. [PubMed: 9027306]
5. Barth M, Schietinger S, Fischer S, Becker J, Nusse N, Aichele T, Lochel B, Sonnichsen C, Benson O. Nanoassembled plasmonic-photonic hybrid cavity for tailored light-matter coupling. Nano Lett. Feb; 2010 10(3):891–895. [PubMed: 20141157]
6. Schmidt MA, Lei DY, Wondraczek L, Nazabal V, Maier SA. Hybrid nanoparticle-microcavity-based plasmonic nanosensors with improved detection resolution and extended remote-sensing ability. Nat Commun. Oct.2012 3:1108-1–1108-7. [PubMed: 23047666]
7. Xu X, Hasan D, Wang L, Chakravarty S, Chen RT, Fan DL, Wang AX. Guided-mode-resonance-coupled plasmonic-active SiO_2 nanotubes for surface enhanced Raman spectroscopy. Appl Phys Lett. May.2012 100:191114-1–191114-5. [PubMed: 22685345]
8. White IM, Gohring J, Fan X. SERS-based detection in an optofluidic ring resonator platform. Opt Exp. Dec; 2007 15(25):17433–17442.
9. Hu M, Fattal D, Li J, Li X, Li Z, Williams RS. Optical properties of sub-wavelength dielectric gratings and their application for surface-enhanced Raman scattering. Appl Phys A. Sep; 2011 105(2):261–266.
10. Cheng C, Scherer A. Fabrication of photonic band gap crystals. J Vac Sci Technol. Nov; 1995 13(6):2696–2700.
11. Round, FE.; Crawford, RM.; Mann, DG. The Diatoms, Biology & Morphology of the Genera. Cambridge, U.K: Cambridge Univ. Press; 1990.
12. Jeffryes C, Solanki R, Rangineni Y, Wang W, Chang CH, Rorrer GL. Electro-luminescence and photoluminescence from nanostructured diatom frustules containing metabolically inserted Germanium. Adv Mater. Jun.2008 20:2633–2637.
13. Gordon R, Losic D, Tiffany MA, Nagy SS, Sterrenburg FA. The glass menagerie: Diatoms for novel applications in nanotechnology. Trends Biotechnol. Feb.2009 27:116–127. [PubMed: 19167770]
14. Jeffeyes C, Campbell J, Li H, Jiao J, Rorrer GL. The potential of diatom nanobiotechnology for applications in solar cells, batteries, and electroluminescent devices. Energy Environ Sci. Sep.2011 4:v3930–3941.
15. Gale DK, Gutu T, Jiao J, Chang CH, Rorrer GL. Photoluminescence detection of biomolecules by antibody-functionalized diatom biosilica. Adv Funct Mater. Mar.2009 19:926–933.
16. Qin T, Gutu T, Jiao J, Chang CH, Rorrer GL. Photoluminescence of silica nanostructures from bioreactor culture of marine diatom nitzschia frustulum. J Nanosci Nanotechnol. Feb.2008 8:2392–2398. [PubMed: 18572654]
17. Yu Y, Addai-Mensah J, Losic D. Synthesis of self-supporting gold microstructures with three-dimensional morphologies by direct replication of diatom templates. Langmuir. Jul.2010 26:14068–14072. [PubMed: 20666460]

18. Losic D, Mitchell JG, Lal R, Voelcker NH. Rapid fabrication of micro- and nanoscale patterns by replica molding from diatom biosilica. Adv Funct Mater. Sep.2007 17:2439–2446.
19. Fuhrmann T, Landwehr S, Rharbi-Kucki ME, Sumper M. Diatoms as living photonic crystals. Appl Phys B-Lasers O. Jan.2004 78:257–260.
20. Ren F, Campbell J, Wang X, Rorrer GL, Wang AX. Enhancing surface plasmon resonances of metallic nanoparticles by diatom biosilica. Opt Exp. Jun; 2013 21(13):15308–15313.
21. Lee PC, Meisel DJ. Adsorption and surface-enhanced Raman of dyes on silver and gold sols. Phys Chem. Aug.1982 86:3391–3395.
22. Liu S, Zhu T, Hua R, Liu Z. Evaporation-induced self-assembly of gold nanoparticles into a highly organized two-dimensional array. Phys Chem. Nov.2002 4:6059–6062.
23. Wustholz KL, Henry AI, McMahon JM, Freeman RG, Valley N, Piotti ME, Natan MJ, Schatz GC, Van Duyne RP. Structure-activity relationships in gold nanoparticle dimers and trimers for surface-enhanced Raman spectroscopy. J Amer Chem Soc. Jul; 2010 132(31):10903–10910. [PubMed: 20681724]
24. Stockman MI, Pandey LN, George TF. Inhomogeneous localization of polar eigenmodes in fractals. Phys Rev B, Condens Matter. Feb; 1996 53(5):2183–2186. [PubMed: 9983705]
25. Mock JJ, Hill RT, Degiron A, Zauscher S, Chilkoti A, Smith DR. Distance-dependent plasmon resonant coupling between a gold nanoparticle and gold film. Nano lett. Jul; 2008 8(8):2245–2252. [PubMed: 18590340]
26. Caldwell JD, Glembocki O, Bezares FJ, Bassim ND, Rendell RW, Feygelson M, Ukaegbu M, Kasica R, Shirey L, Hosten C. Plasmonic nanopillar arrays for large-area, high-enhancement surface-enhanced Raman scattering sensors. ACS Nano. Apr; 2011 5(5):4046–4055. [PubMed: 21480637]
27. Sun G, Khurgin JB. Origin of giant difference between fluorescence, resonance, and nonresonance Raman scattering enhancement by surface plasmons. Phys Rev A. Jun; 2012 85(6):063410-1–063410-8.

Biographies

Fanghui Ren (S′12) received the B.S. degree in physics from Southwest University, Chongqing, China, in 2010, and the M.S. degree in electrical and computer engineering from Oregon State University, Corvallis, in 2012. She is currently working toward the Ph.D. degree in electrical and computer engineering at Oregon State University, Corvallis, OR, USA. Her research interests include hybrid biological-plasmonic optical sensors, photonic crystal, and surface plasmonic devices for optical communication.

Jeremy Campbell received the B.S. degree in chemical engineering from Oregon State University, Corvallis, in 2006, and the M.S. degree in chemistry from the University of Oregon, Eugene, in 2009. He is currently working toward the Ph.D. degree in chemical engineering at Oregon State University, Corvallis, OR. His research interests include the optical properties of diatom biosilica for solar energy conversion and strategies for biological thin film formation for engineering applications.

Gregory L. Rorrer received the B.S. degree in chemical engineering from the University of Michigan, and the Ph.D. degree in chemical engineering from Michigan State University. He is currently a Professor and the Head of the School of Chemical, Biological, and Environmental Engineering, Oregon State University, and holds the James & Shirley Kuse Chair in chemical engineering. From 2009 to 2011, he served as the Program Director of the Energy for Sustainability program within the Engineering Directorate at the National Science Foundation (NSF). His expertise encompasses bioprocess engineering, renewable

energy and fuels, microchannel reactors, and biological fabrication of nanomaterials. His current research interests include harnessing the unique biosynthetic capacities of photosynthetic algae for applications in nanotechnology, bioenergy, bioactive compound production, and environmental remediation. He is also a coauthor on the 4th and 5th editions of the widely-used textbook *Fundamentals of Momentum, Heat, and Mass Transfer*.

Alan X. Wang received the B.S. degree from Tsinghua University and the M.S. degree from the Institute of Semiconductors, Chinese Academy of Sciences, Beijing, China, in 2000 and 2003, respectively, and the Ph.D. degree in electrical and computer engineering from the University of Texas at Austin in 2006. He has been an Assistant Professor in the School of Electrical Engineering and Computer Science, Oregon State University since 2011. From 2007 to 2011, he was a Research Scientist at Omega Optics, Inc. He has authored or coauthored more than 40 journal papers, and more than 50 conference papers. He holds 3 U.S. patents. His research interest covers board level optical interconnects, micro- and nano-photonic devices, RF photonics, and optical sensing technologies including IR spectroscopy and Raman scattering for biomedical research and environmental protection. He is a member the Optical Society of America and the International Society for Optical Engineering. He served as a program committee member and session chair for SPIE Photonic West conference in Optoelectronic Interconnects and Component Integration XI from 2009 to 2011, and conference chair for Photonics Asia in 2010.

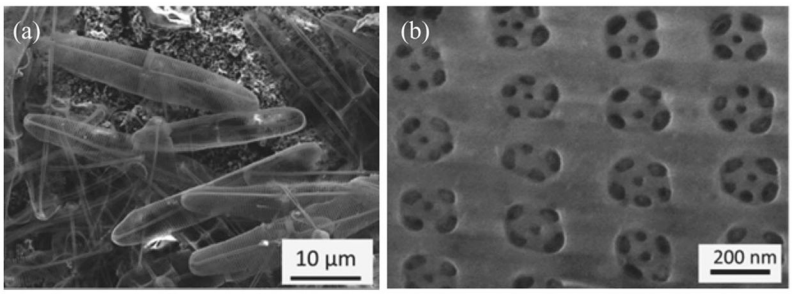

Fig. 1.

Representative SEM images of *Pinnularia* sp. showing (a) an overview of diatom frustules and (b) nanoscale arrays of primary pores on a frustule with 50–80 nm subpores.

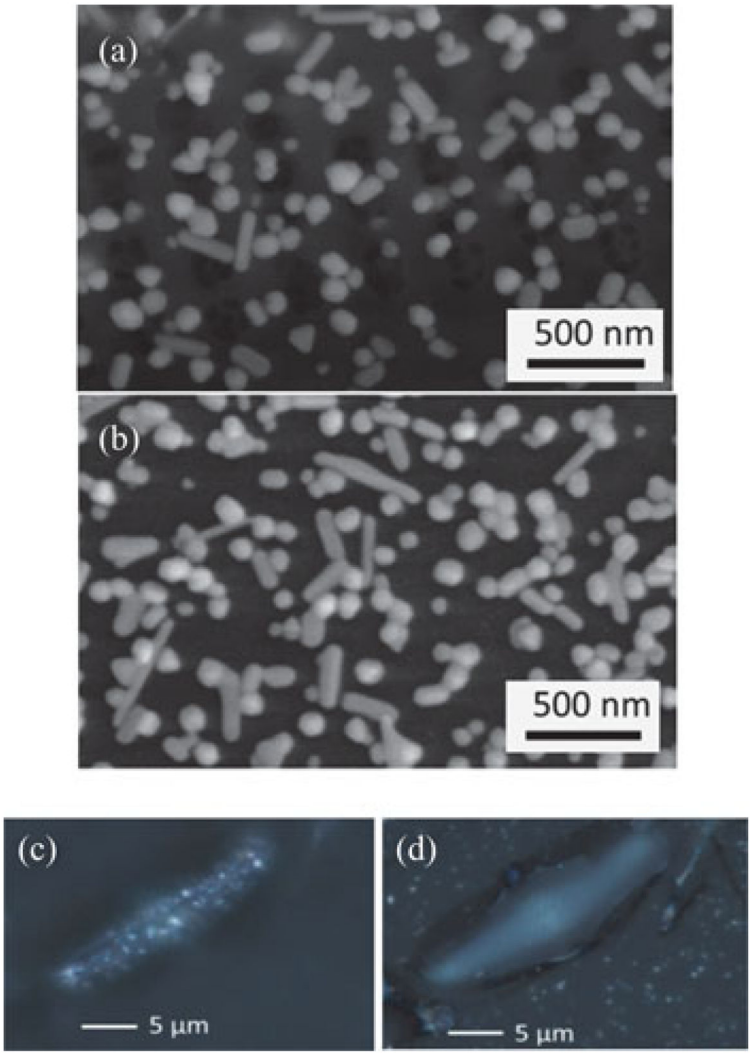

Fig. 2.

(a) SEM image of Ag NPs on the diatom frustule. (b) SEM image of Ag NPs on the glass substrate. (c) Optical image of Ag NPs on a diatom frustule with focal plane at the diatom surface. (d) Optical image of Ag NPs with focal plane on the glass substrate.

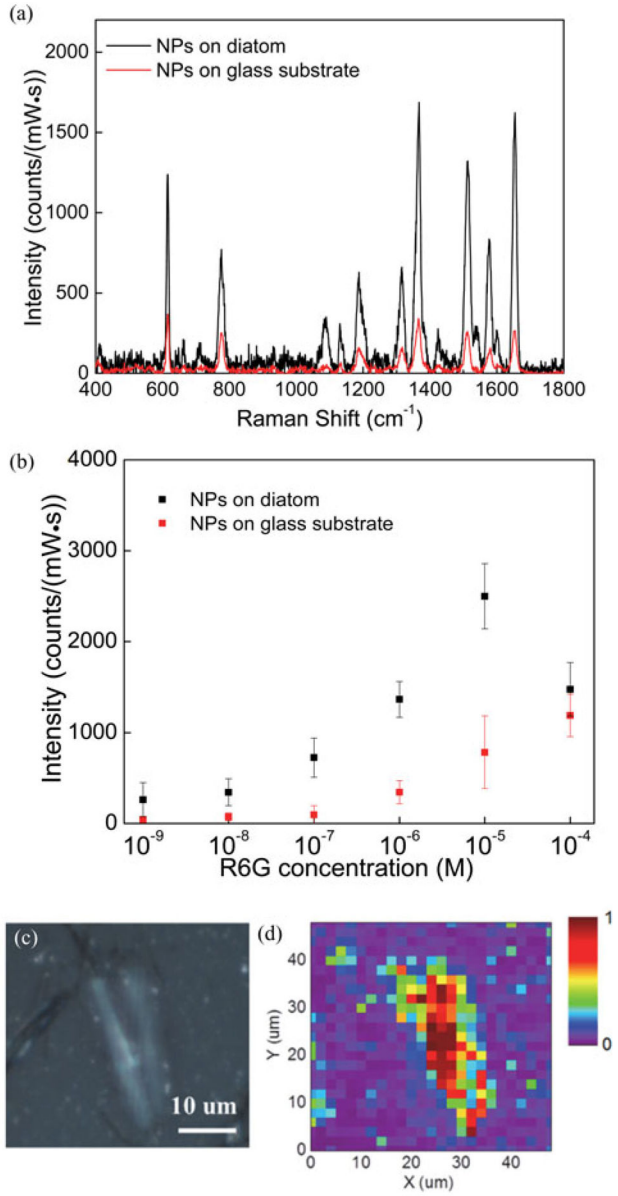

Fig. 3.

(a) SERS spectra of 1 μM R6G coated on Ag NPs-on-diatom (black) and Ag NPs-on-glass (red). (b) Intensities of Raman band at 1368 cm^{-1} for different R6G concentrations. (c) Optical image of the sensing area scanned for SERS enhancement and (d) mapping of Raman signal intensity at 1368 cm^{-1}. During the measurement, the excitation power was set at 1.2 mW and integration time was 1 s.

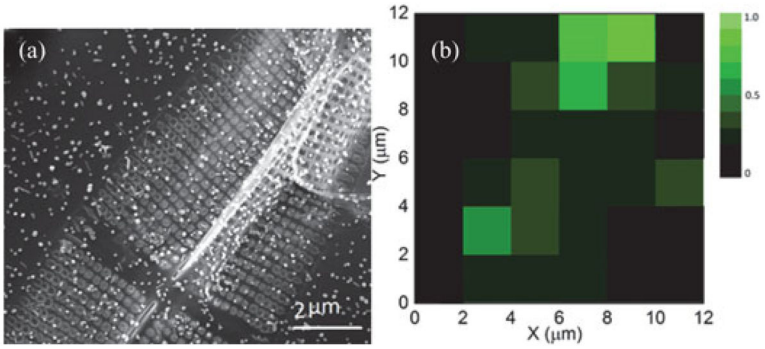

Fig. 4.

(a) SEM image of the acquisition area for SERS mapping. (b) The map of Raman signal intensity at 1368 cm^{-1} normalized by the NP numbers in each grid showing in the SEM image. The excitation power was set at 1.2 mW and the integration time was 1 s.

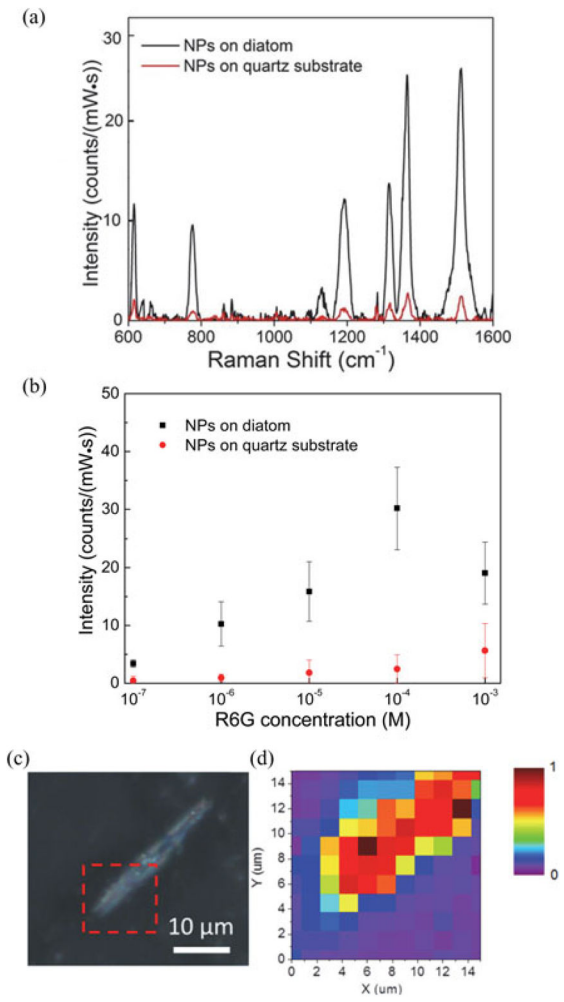

Fig. 5.

(a) SERS spectra of 100 μM R6G coated on Ag NPs-on-diatom (black) and Ag NPs-on-quartz (red), (b) Intensities of Raman band 1368 cm^{-1} for different R6G concentrations. (c) Optical image of the area scanned for SERS measurement, and (d) map of Raman signal intensity at 1368 cm^{-1}. During the measurement, the integration time was 60 s and the grating groove density was set at 300/mm. The excitation power was 2.1 mW.

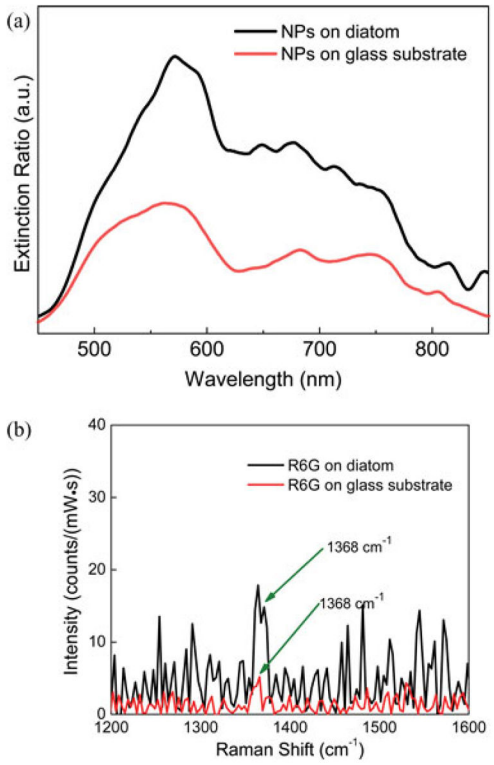

Fig. 6.

(a) Measured extinction spectra of NPs on a diatom frustule (black) and Ag NPs on a glass substrate (red). (b) Raman spectra of 5 mM R6G on diatom (black) and glass substrate (red). During the Raman measurement, the excitation power was set at 1.2 mW and integration time was 5 s.